MAPPING COASTAL UPWELLING SYSTEMS OVER TIME: AN AUTOMATED HIGH-RESOLUTION SEGMENTATION OFF THE CALIFORNIA COAST

Brian Amaro

Stanford University

ABSTRACT

Coastal upwelling occurs when deep, nutrient rich ocean water is able to reach the surface near a coast. The ecosystems that develop from the nutrient-rich water are quite productive and changes to them can have significant environmental and economic impacts. Mapping the extent of upwelling systems can help us better understand the distribution of upwelling systems in order to inform models that often cannot reproduce coastal upwelling accurately. This in turn can help with making advances for predicting the locations and extents of upwelling events. Building off of techniques that have been applied to other geographical regions, the work from this study automatically maps the upwelling system off the California coast at high temporal and spatial resolution from 2015 to 2022.

In this work, detection of upwelling events was based on the 8-day MODIS Sea Surface Temperature data at a 4 kilometer resolution. A modified version of the topographic position index algorithm was utilized to segment areas that were significantly colder than their surroundings. This method was validated through the comparison of the upwelling locations mapped by the algorithm with maps of other upwelling-induced features and verifying expected characteristics of the upwelling systems, including showing an increased chlorophyll-a concentration from the expected nutrient-rich waters that are characteristic of upwelling.

1. INTRODUCTION

Coastal upwelling systems are locations where cold and nutrient-rich waters rise from the depth of the ocean, replacing surface waters that are transported away from the shore from equatorward alongshore winds as regulated by Ekman dynamics. Due to the upwelling found there, the California Current System (CCS) is "among the most productive ecosystems in the global ocean. It has been suggested that eastern boundary current systems [such as the CCS] cover less than 2% of the global ocean surface, but contribute ~7% of the global primary production and more than 20% of the global fish catches" (Xiu et al., 2018). Studying these upwelling zones therefore allows us to understand how they may change in the future which can have important environmental and economic implications for the systems that depend on the upwelling process.

Historically, upwelling has been measured using monthly mean surface atmospheric pressure data. Indices such as the Bakun index aim to quantify upwelling by measuring the source winds. However, the requirement of a wind measuring instrument limited the area that Bakun's study could cover (1973). Other methods also involve field studies such as (Roughan, 2005) which collected hydrographic data on a 1 day cruise with radar measurements to study upwelling around Point Loma, California. Using in-situ measurements makes it more difficult for methods to be applied globally as the data is often not readily accessible around the world

In recent decades, remote sensing data has been increasingly used to study upwelling. For example, it has been used in studies that focus on the temporal variability of upwelling with localized long time series analyses such as this 60-year study off the Portuguese coast (Leitão et al., 2019) that used sea surface temperature data from Advanced Very High Resolution Radiometer (AVHRR), as well as this 26 year study that combined wind and SST data "to delineate oceanographic seasons based on upwelling regimes" (Goela et al., 2016). Remote sensing data has also been used in efforts that focus on the mapping of coastal upwelling in order to understand the spatial variability in addition to the temporal variability. One such study

was conducted by Huang et al to map upwelling systems of the Australian southeastern coast over 14 years using monthly MODIS SST data (Huang & Wang, 2019). There is also this study that maps coastal upwelling east of Taiwan with a higher temporal resolution of daily SST data from the Himawari-8 geostationary satellite over a shorter time period of 5 years and a smaller area (Huang et al., 2021).

However, while there have been efforts to map upwelling over time, methods are still being developed and have been applied to only a few regions across the globe. This project therefore develops a method that uses data from global satellites and thus can be applied to other locations. This method is also using data that at a high enough temporal resolution of 8 day periods to capture coastal upwelling events that only have a length on the magnitude of days to weeks as shown in Huang et al., 2021. This method is also open-source with the source code available in the supplementary material in the appendix in order to readily enable the development of the method by the scientific community.

2. METHODOLOGY

2.1 DATA

To map coastal upwelling, the algorithm utilized mapped Aqua Moderate Resolution Imaging Spectroradiometer (MODIS) 11 micrometer sea surface temperature data. To validate the algorithm, Aqua MODIS chlorophyll-a concentration data was utilized. Both of these datasets had observations that represented an 8-day period and had a 4 kilometer spatial resolution. The time range of these datasets were from January 1st, 2015 to December 31st, 2022 and thus each included 366 images. Both datasets were pulled from NASA's EarthData Ocean Color Database. While global data was extracted from the database, all images were then cropped to the study area of the California coastline. Specifically, the images were cropped so that the resulting data laid between 33° N and 42° N in terms of latitude and between 117° W

and 127° W in terms of longitude. This allowed the entire California coast to be included in the dataset.

An example of an image in the dataset can be seen in Figure 1 which showcases sea surface temperature from September 5th, 2016 to September 12th, 2016. This image depicts several upwelling zones as shown by the low temperature areas off the coast. The image also shows some missing data in the bottom left and bottom center of the images that come from occlusions from cloud cover. This is not uncommon in 8-day period data and the effects are discussed when evaluating the algorithm.

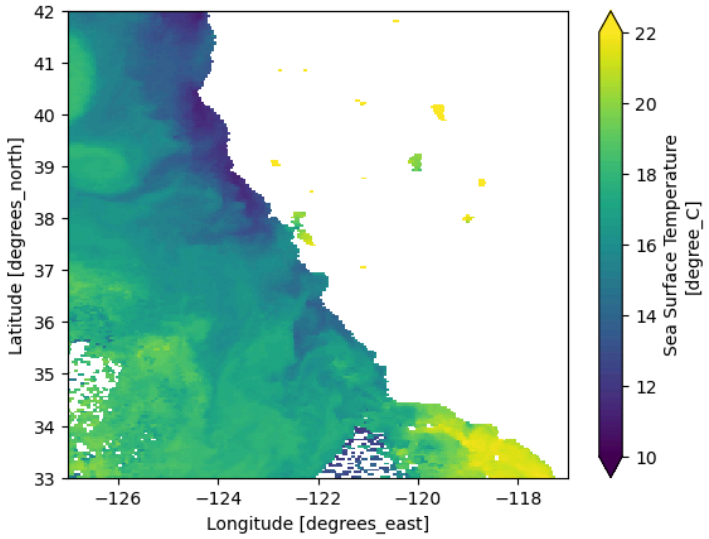

Figure 1. Sea surface temperature composite showing 8-day average data from September 5th, 2016 to September 12th, 2016.

2.2 TOOLS

A variety of tools were utilized in order to enable the creation and presentation of the algorithm. The programming language Python, particularly the numpy and xarray packages, were used to process the data from the individual NetCDF files. The programming language R, particularly the ggplot package in the tidyverse collection, was used to analyze and quantitatively visualize the processed data. Python, namely the matplotlib package, and Adobe Photoshop were

used to create the time lapse animations that can be found in the supplementary materials in the appendix.

2.3 ALGORITHM PIPELINE

The algorithm processes one 8-day period at a time and then compiles all of the processed data into a dataframe. The processing pipeline starts by cropping the global SST and chlorophyll-a data to encompass a rectangle centered on the California coast as specified in the data section. An additional crop is then done on both SST and chlorophyll-a data to mask out the data that would be used for further calculations. This mask encompasses a narrower, non-rectangular region of coastline that more accurately depicts the coast. The latitude and longitude boundaries of this mask can be found in the appendix.

The algorithm then maps the upwelling zones based on the SST data using two different methods. The first method utilized is the naive method, in which the algorithm marks any pixel that has a temperature lower than 13 °C, a value selected as a representative value of upwelling based on manual tuning that was based on references to literature such as Dabuleviciene et al. (2023), as an upwelling zone. The second is the Topographic Position Index (TPI) method. This method is typically used with elevation data to find hills and valleys. However, studies such as Huang and Feng (2015) have shown that TPI can also be used with SST data to find pixels that have a lower temperature than their surrounding neighbors (i.e. locations of a local SST anomaly). The following equation is used to calculate TPI from SST data:

$$TPI(x, y) = SST(x,y) - WD(x,y)$$

where x and y are the positions of a pixel and WD is the average SST within a window of neighboring pixels (Huang and Feng, 2015). In this study, the algorithm utilizes a square window with a side length of 25 pixels. An example of a map is shown below in Figure 2.

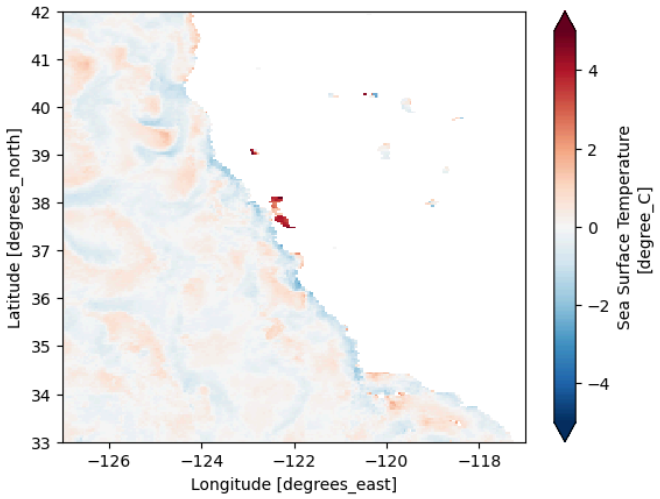

Figure 2. A Topographic Position Index for SST map. The blue regions indicate a negative local SST anomaly, a characteristic that would be expected of an upwelling zone.

In the TPI method, the algorithm marks the pixels that have a TPI value between -5 and -1 as upwelling zones. These values were selected empirically – the higher bound of -1 was chosen to prevent false negatives, and the lower bound was chosen of -5 to exclude values that generally were caused by missing data from cloud coverage.

Having the upwelling zones demarcated, the algorithm calculates several statistics on four different areas: the overall rectangle of data as shown in Figure 1, the coastal mask of data, the upwelling zones demarcated by the naive method, and the upwelling zones demarcated by the TPI method. This is done to compare if each area has the expected differences characteristic of upwelling zones. The characteristics calculated are: area in pixels, average sea surface temperature, and average of chlorophyll-a concentration. One should note that the SST and the chlorophyll-a averages are area-weighted averages that correct for the fact that the area that a pixel represents decreases as their latitude increases above the equator.

3. RESULTS

The mapped upwelling zones for both the naive method and the TPI method for the entire diagram can be seen in the time lapse animations included in the supplementary materials in the appendix. The results are further summarized in the three following graphs of Figures 3, 4, and 5.

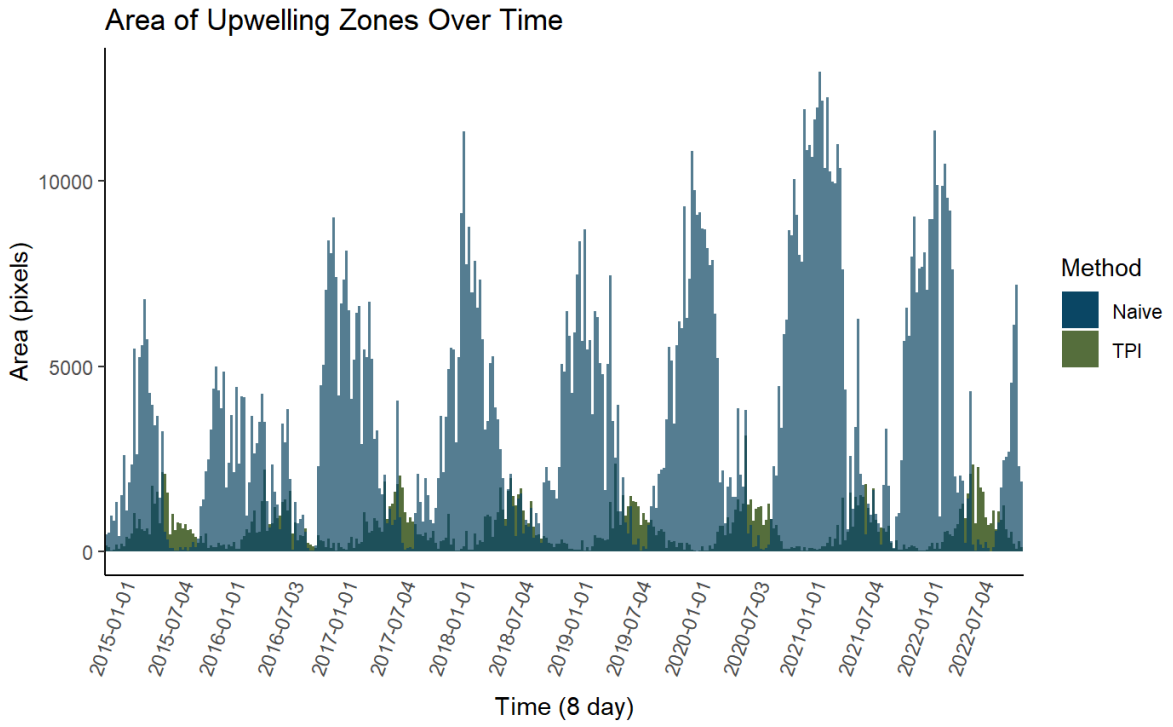

Figure 3. This graph shows how the area of the delineated upwelling zones has changed over time. The values from the naive method are superimposed on top of the values from the TPI method.

Figure 3 shows the area of upwelling zones over time in pixels. The area of the upwelling zone mapped by the naive method oscillates with maximums in the winter and minimums in the summer while the area of the upwelling zone mapped by the TPI method inversely oscillates with maximums in the summer and minimums in the winter. The area of the upwelling zone mapped by the naive method is also generally much larger than the area of the upwelling zone

mapped by the TPI method. The area of the upwelling zone mapped by the naive method also appears to have a longer period oscillation with a general increase in area from 2015 to 2021 and decrease afterwards.

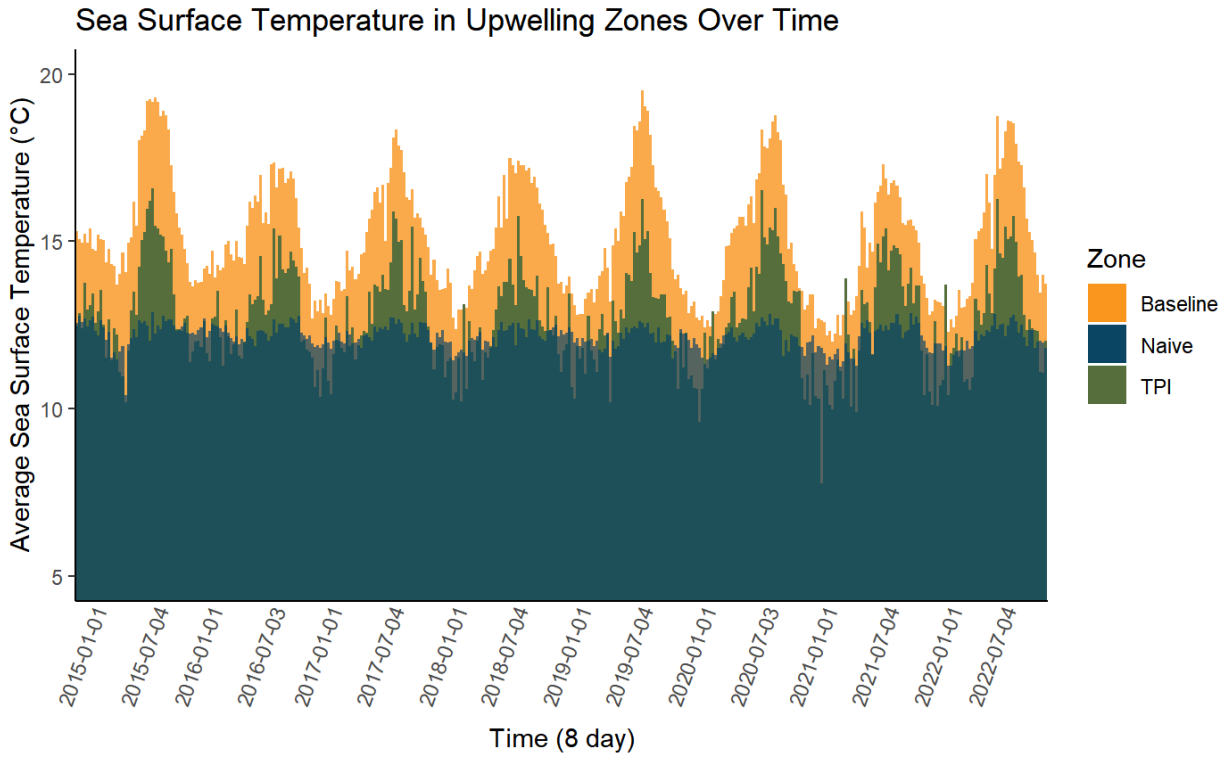

Figure 4. This graph shows how the average SST in the baseline area and the upwelling zones demarcated by the naive and TPI methods changes over time. Note that the baseline area corresponds to the entire study area as depicted by Figure 1 as well as that the graph showcases the data for the three areas superimposed on each other.

Figure 4 shows average SST in three different areas over time. Additionally, the average SST in the baseline and in the TPI area reaches clear maximums in the summer and minimums in the winter. The average SST in the naive area does as well but to a much lesser extent. Notably, the average SST of the baseline area is always greater than the average SST of the upwelling zones from both the naive and TPI methods.

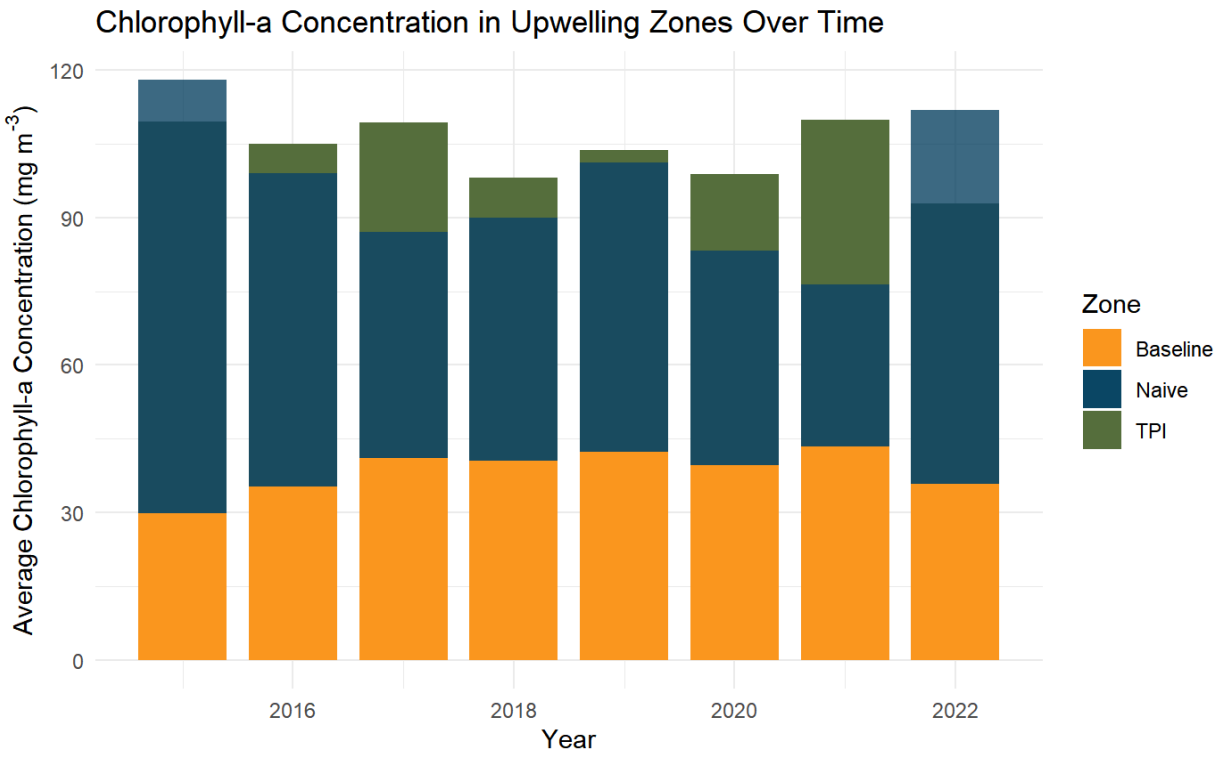

Figure 5. This graph shows how the average chlorophyll-a concentration in the baseline area and the upwelling zones demarcated by the naive and TPI methods changes over time. Note that, similar to Figure 4, the baseline area corresponds to the entire study area as depicted by Figure 1 as well as that the graph showcases the data for the three areas superimposed on each other.

Figure 5 depicts average chlorophyll-a concentration in the different areas over time. The data is grouped per year as the 8-day groupings showed significant noise which made it more difficult to see the overall trend. The average chlorophyll-a concentration in the baseline area is significantly lower than the average chlorophyll-a concentration in the upwelling zones demarcated by either method. The average chlorophyll-a concentration in the upwelling zones, particularly as defined by the naive method, shows some temporal variation, but the pattern is unclear due to the limited timespan of the study relative to the variation.

4. DISCUSSION

Figure 3 shows the biases present in both methods. The naive method's maximums temporally corresponding to the winter seasons is a product of the absolute temperature threshold found in the naive method. Winter simply has greater areas that have colder temperature, which does not necessarily come from upwelling zones getting larger but rather from colder atmospheric temperatures and general sea surface temperatures. This implies that the naive method has significant false positives. The TPI method's maximums temporally corresponding with the summer seasons is also likely a product of the method's thresholding. Since a negative TPI indicates that the pixel is colder than surrounding pixels, there is more likely to be marked upwelling zones (defined by having a negative TPI) when the surrounding water is warmer as in the summer. This indicates that the TPI method may have some false negatives in the winter as it may not be detecting upwelling events in the colder months due to the smaller difference in SST.

Despite these biases, Figure 4 and Figure 5 help validate the algorithm's accuracy. We expect that, due to the defining influx of cold deep ocean water, upwelling zones would have a lower temperature than areas that are not upwelling zones. This in fact holds for the zones demarcated by both the naive and TPI methods as showcased in Figure 4. One must note that a lower SST in the marked upwelling zones was to be expected, as both methods are defined by having a low SST (absolutely or relatively). Figure 5 further validates the algorithm with a similar framework but with another dataset: chlorophyll-a concentration. We expect, due to the fact that the deep ocean water that is being upwelled is nutrient rich, therefore leading to an increase in phytoplankton production and consequently chlorophyll-a concentration (Xiu et al., 2018). Figure 5 shows that this holds true for the zones outlined by both the naive and TPI methods. This is significant as chlorophyll-a concentration was not used in the algorithm in the delineating of the upwelling zones and therefore serves as an independent validation.

There are some data limitations that also affected the results. As can be seen in the timelapses, cloud coverage skewed the detections of upwelling zones. It qualitatively appears that the main effect is not so much that the clouds are obscuring upwelling zones, but rather that clouds cause the immediately adjacent areas to have a lower SST. This is likely due to the fact that those areas were in the shadow of the clouds for some time and therefore received less solar radiation. This can potentially cause both methods to detect false positives in these cloudy areas; this is particularly an issue for the TPI method as clouds are creating local cold SST anomalies.

5. CONCLUSION

In order to allow us to better understand the variability of upwelling systems, this study created an algorithm that can outline upwelling areas. While the parameters have been tuned for the region of study of the California coast, the algorithm uses globally available data and therefore can be applied anywhere. An accompanying dataset has also already been produced as well that can be used for further studies to study the spatial and temporal distribution of upwelling off the California coast. This study has also further developed a framework to validate the upwelling zone outlining method using chlorophyll-a data that can be readily applied to other methods as well.

Of the two upwelling zone outlining methods this study utilized, the TPI method appears to be significantly less biased than the naive method. However, it still has its limitations such as its difficulties in detecting upwelling in the winter seasons.

Future studies could look at ways to improve the algorithm such as adding constraints that ensure a degree of clustering such that outlined upwelling zones are more continuous. This would likely help alleviate some of the issues caused by cloud coverage as false positive detections from clouds are often disconnected from the true coastal upwelling zones.

Further studies can also apply the same validation framework this study used with chlorophyll-a data to find other approaches of validating the upwelling outlining methods using

other datasets as proxies for other characteristics of upwelling. Wind strength and direction, for example, is an initial promising candidate for such a study.

The hope is that this method will contribute to bettering our understanding of coastal upwelling systems and the ecosystems they create. With changing climate conditions affecting systems across our planet, it is best to understand how they have changed in the past to see what light that might shine on their future.

6. REFERENCES

Bakun, A. (1973). Coastal upwelling indices, west coast of North America. US Department of Commerce. NOAA Technical Report, NMFS SSRF-671

Dabuleviciene, T., Jucevicius, D., Zolubas, T., Vaiciute, D., & Nika, N. (2023). The Effect of Short-Term Upwelling Events on Fish Assemblages at the South-Eastern Coast of the Baltic Sea. *Water*, *15*(3), 452. https://doi.org/10.3390/w15030452

Goela, P. C., Cordeiro, C., Danchenko, S., Icely, J., Cristina, S., & Newton, A. (2016). Time series analysis of data for sea surface temperature and upwelling components from the southwest coast of Portugal. *Journal of Marine Systems*, *163*, 12–22. https://doi.org/10.1016/j.jmarsys.2016.06.002

Huang, Z., Hu, J., & Shi, W. (2021). Mapping the Coastal Upwelling East of Taiwan Using Geostationary Satellite Data. *Remote Sensing*, *13*(2), 170. https://doi.org/10.3390/rs13020170

Huang, Z., & Wang, X. H. (2019). Mapping the spatial and temporal variability of the upwelling systems of the Australian south-eastern coast using 14-year of MODIS data. *Remote Sensing of Environment*, *227*, 90–109. https://doi.org/10.1016/j.rse.2019.04.002

L3 Browser - NASA Ocean Color. (n.d.). Oceancolor.gsfc.nasa.gov. https://oceancolor.gsfc.nasa.gov/l3/

Leitão, F., Baptista, V., Vieira, V., Laginha Silva, P., Relvas, P., & Alexandra Teodósio, M. (2019). A 60-Year Time Series Analyses of the Upwelling along the Portuguese Coast. *Water*, *11*(6), 1285. https://doi.org/10.3390/w11061285

Roughan, M. (2005). Observations of divergence and upwelling around Point Loma, California. *Journal of Geophysical Research*, *110*(C4). https://doi.org/10.1029/2004jc002662

Xiu, P., Chai, F., Curchitser, E. N., & Castruccio, F. S. (2018). Future changes in coastal upwelling ecosystems with global warming: The case of the California Current System. *Scientific Reports*, *8*(1). https://doi.org/10.1038/s41598-018-21247-7

7. APPENDIX

Supplementary materials are hosted in the following Github

Geographic coordinates of the mask defining the coast.

Latitude Range (° N)	Longitude Range (° W)
38-42	126-123
36-38	125-121
35-36	124-120
32-35	123-116